I&EC research
Industrial & Engineering Chemistry Research

Article

pubs.acs.org/IECR

# Enhancement of the Partial Oxidation of Methanol Reaction over CuZn Catalyst by Mn Promoter

Kuan-Yi Lee,[†] Chia-Chieh Shen,[‡] and Yuh-Jeen Huang*[,†]

[†]Department of Biomedical Engineering & Environmental Sciences, National Tsing Hua University, Hsinchu 30013, Taiwan
[‡]Department of Mechanical Engineering, Yuan Ze University, Chungli 32003, Taiwan

Supporting Information

**ABSTRACT:** A series of in situ experiments on mechanisms and top-down LHHW (Langmuir−Hinshelwood−Hougen−Watson) microkinetic analysis were conducted for the partial oxidation of methanol on CuMnZn (ca. 28.0 wt % Cu, 23 wt % Mn, and 49 wt % Zn) catalyst. In comparison with CuZn (ca. 29 wt % Cu and 71 wt % Zn), CuMnZn catalyst with the structure of copper−manganese spinel $CuMn_2O_4$ enhanced the turnover frequency (TOF) for methanol conversion at a lower temperature (from 4.2 to 10.1 $s^{-1}$ at 150 °C). Mn also played a role in electronic charge transfer, which could enhance formate decomposition and mitigate the accumulation of carbonate species at high temperature. From a kinetic modeling analysis, the activation energy of CuZn-based catalyst was apparently reduced from 22.4 to 16.5 kcal/mol by the Mn promoter.

## 1. INTRODUCTION

The catalytic partial oxidation of methanol (POM) has been extensively studied during the past decade.[1−8] POM, an exothermic reaction, has the advantage of starting up quickly and not requiring a heat supply if the reaction reaches steady state.[9−11] Hydrogen, the primary product of the POM reaction, is supplied to proton-exchange membrane fuel cells (PEMFCs), which have been extensively studied because of their attractive properties, such as high power, low emissions, and low operating temperature in the fuel cell system.

Copper-containing catalysts, especially CuZn-based oxides, have usually been used in the methanol reforming reaction. CuZn catalysts display a high initiation temperature of $T_i \approx 180$ °C and a high selection and activity at temperatures higher than 200 °C. We reported previously that the concentration of oxygen can affect not only the MeOH conversion and selectivity, but also the Cu state.[12] Some authors[13,14] reported identifying $Cu^0$ and $Cu^+$ as possible active centers; however, the Cu state would change dynamically with the methanol synthesis or decomposition conditions.[15,16]

Manganese oxides are reported as one of the most efficient transition-metal compounds in catalytic reactions[17,18] and are considered environmentally friendly materials. In addition, copper−manganese catalysts have been successfully applied in many catalytic reactions, such as CO oxidation,[19] the water−gas shift reaction (WGSR),[20,21] the steam reforming of methanol (SRM),[22,23] and the total oxidation of propane and ethanol.[18] Amorphous copper manganite ($CuMn_2O_4$), well-known as "hopcalite", is an efficient catalyst. Kanungo[24] ascribed the "anomalous promotion" of hopcalite to the formation of copper−manganese spinel $CuMn_2O_4$, which can be more precise for electronic charge transfer between copper and manganese cations within the spinel lattice. It enhances the catalytic activity when $Mn^{3+}$−$Mn^{4+}$ is coupled in the structure of the oxide.[25] Manganese oxides were introduced into the CuZn-based catalyst in this study to enhance the POM reaction at low temperature.

The overall reaction for the partial oxidation of methanol is

$$CH_3OH + \frac{1}{2}O_2 \rightarrow 2H_2 + CO_2 \quad (1)$$

However, multiple reactions in the POM can occur simultaneously, and many intermediates can be involved.[26] Some mechanisms for POM seem to agree with other reactions, such as methanol decomposition (MD), the steam reforming of methanol (SRM), and the water−gas shift. Peppley et al.[27] proposed that methoxide is rapidly formed and that the rate-determining step (RDS) is the cleavage of the C−H bond to form the surface-bonded $H_2CO$ species for MD and the SRM; however, the RDS for the WGSR is the formation of formate species. Some authors[6,7,28,29] have proposed the first reaction step as methanol O−H bond activation with the formation of surface methoxide species

$$CH_3OH \rightarrow CH_3O^* + H^* \quad (2)$$

$$CH_3OH + O^* \rightarrow CH_3O^* + OH^* \quad (3)$$

Subsequently, the spillover of hydrogen would take place between the Cu and metal oxides to form chemisorbed hydrogen, chemisorbed hydroxy, formaldehyde, and methoxy species

$$CH_3O^* + O^* \rightarrow CH_2O^* + OH^* \quad (4)$$

$$CH_2O^* \rightarrow CHO^* + H^* \quad (5)$$

Then, the formate would be produced on the surface

$$CHO^* + O^* \rightarrow CO_2H^* \quad (6)$$

**Received:** March 10, 2014
**Revised:** July 20, 2014
**Accepted:** July 23, 2014
**Published:** July 23, 2014





dx.doi.org/10.1021/ie501023z | Ind. Eng. Chem. Res. 2014, 53, 12622−12630

Finally, gas-phase CO, $CO_2$, and $H_2$ are released from the surface by the decomposition of formate or methoxy species. Although previous works have shown that many mechanisms exist for the POM, fewer have been published concerning the influence of the states of the catalysts and absorbed species.[30]

In the work presented here, CuZn-based catalyst promoted by manganese was prepared by a coprecipitation method and investigated in the partial oxidation of methanol (POM) reaction. We characterized the change in the states of copper and manganese oxide species during the POM reaction by in situ X-ray absorption spectroscopy and inferred the mechanisms by in situ diffuse-reflectance infrared Fourier transform spectroscopy (DRIFTS). Moreover, the kinetic model set of the Langmuir−Hinshelwood−Hougen−Watson (LHHW) formalism[31] was derived based on a steady-state analysis of the final surface mechanisms.

## 2. EXPERIMENTAL SECTION

**2.1. Catalyst Preparation.** Copper-based catalysts, namely, Cu/ZnO (CuZn) (ca. 29.2 wt % Cu and 70.8 wt % Zn) and Cu/Mn/ZnO (CuMnZn) (ca. 28.0 wt % Cu, 23.3 wt % Mn, and 48.7 wt % Zn), were prepared by the coprecipitation of metal nitrates in aqueous solution. Suitable amounts of $Cu(NO_3)_2$, $Zn(NO_3)_2$, and $Mn(NO_3)_2$ were mixed well in 600 mL of deionized water at 70 °C. The solution containing metal cations in the required proportions was stirred rapidly and quickly added to a 2 M $Na_2CO_3$ solution until the metal salts were precipitated at pH 7. Vigorous stirring was maintained at 70 °C. After aging to pH 8, the CuMnZn precipitates were filtered, washed thoroughly with deionized water, and then dried at 105 °C overnight. The final catalysts were calcined in air at 400 °C for 4 h to yield fresh oxidized CuMnZn samples.

**2.2. Characterization.** The exact compositions of the catalysts were analyzed by inductively coupled plasma (ICP) mass spectrometry (Perkin-Elmer, SCIEX ELAN 5000).

The structure of the catalysts, except fresh CuMnZn, was characterized by X-ray powder diffraction (XRD, Rigaku TTRAX III diffractometer) using Cu K$\alpha$ ($\lambda$ = 0.15406 nm) radiation. The scanning of 2$\theta$ angles ranged from 20° to 80° at a rate of 4° $min^{-1}$. The XRD spectrum of fresh CuMnZn catalyst was measured at the BL01C2 beamline of the National Synchrotron Radiation Research Center (NSRRC), Hsinchu, Taiwan, with a wavelength of 16 keV and an exposure time of 300 s.

To study the changes in the states of copper and manganese species during the POM reaction, in situ X-ray absorption spectroscopy (XAS) analysis of catalysts was conducted at the 17C beamline of the National Synchrotron Radiation Research Center (NSRRC), Hsinchu, Taiwan. The electron storage ring was operated at 1.5 GeV with a stored current of 200 mA in a top-up injection mode. A Si(111) double-crystal monochromator was used to select the energy, with an energy resolution ($\Delta E/E$) of 1.9 × $10^{-4}$. Absorption at the Cu K-edge (8.979 keV) and Mn K-edge (6.539 keV) was measured in transmission mode. All data were analyzed using WinXAS 3.0 and were Fourier transformed on $k^3$-weighted oscillations in the range of 2.8−10 $Å^{-1}$. Other detailed information was presented in a previous study.[12]

The variations of species on the surface of the catalyst were recorded by infrared spectroscopy (Thermo Scientific Nicolet 6700) with a DRIFT accessory (Harrick) and a mercury cadmium telluride (MCT/A) detector. About 1.0 g of the catalyst was packed in the sample holder of the in situ cell and subsequently heated by a thermostatically controlled process. After the reaction gas ($CH_3OH$ and $O_2$/Ar, with an $O_2$/$CH_3OH$ ratio of 0.5) had been fed for 15 min at various temperatures (160, 180, 200, and 300 °C), all samples were purged with nitrogen (>99.99%) for 10 min to remove reversibly adsorbed species. The spectra were collected at a resolution of 4 $cm^{-1}$ and an accumulation of 32 scans.

**2.3. Catalytic Test.** Catalytic activity measurements were carried out in a fixed-bed reactor operating at atmospheric pressure. The catalysts were pressed and sieved into 60−80 mesh, and 100 mg of catalyst was placed into a quartz tube (inner diameter, 4 mm) stabilized by quartz wool at both ends. A thermocouple was located in the center of the catalyst bed to control the reaction temperature. Liquid feed ($CH_3OH$, Macron, >99.9%) and gaseous feed (oxygen, >99.99%; Ar, >99.99%) were introduced by piston pumps and a Brooks 5850E mass flow controller, respectively. The molar ratio of oxygen to methanol (O/M) was controlled at 0.5. Samples were collected in two sampling loops and sent to a gas chromatograph (China GC 2000) equipped with Porapak Q and molecular sieve 5A columns and two thermal conductivity detectors and a flame ionization detector in parallel for analysis of $H_2$, CO, $CO_2$, $O_2$, $CH_3OH$, and $H_2O$. Catalytic activation of the catalysts was evaluated in terms of turnover frequency (TOF, $s^{-1}$), which is the rate of the MeOH conversion ($n_{MeOH,in} - n_{MeOH,out}$) per second, normalized by the number of active copper surface atoms. The number of moles of active copper surface atoms was calculated from the Cu dispersion multiplied by the total copper loading. Hydrogen selectivity ($S_{H_2}$) and CO selectivity ($S_{CO}$) are defined as $S_{H_2} = n_{H_2}/(n_{H_2} + n_{H_2O}) \times 100\%$ and $S_{CO} = n_{CO}/(n_{CO} + n_{CO_2}) \times 100\%$. The weight hourly space velocity (WHSV) and gas hourly space velocity (GHSV) were set at 9.48 and 60000 $h^{-1}$, respectively.

**2.4. Microkinetic Modeling Analysis.** All catalysts were sieved to 60−80 mesh. The feed reactants contained approximately 90% $N_2$ balanced with $O_2$/$CH_3OH$ in a ratio of 0.5. Kinetic data were collected for CuMnZn catalyst at temperatures of 160−190 °C and for CuZn catalyst at 170−200 °C at varying contact times ($W/F$) of 2.03−7.29 $kg_{cat}$ s $mol_{MeOH}^{-1}$. All kinetic data were collected to ensure that deactivation did not affect the rate, and the kinetic experiments were carried out in the absence of mass- and heat-transfer limitations, as confirmed by the Koros−Nowak (KN) criterion test.[32,33] Mass balances on carbon and oxygen were always satisfied within ±10%. Parameters were estimated by nonlinear regression using Athena Visual Studio[34] based on the criterion of the least residual sum of squares (RSS).

## 3. RESULTS AND DISCUSSION

**3.1. Characteristics of CuZn and CnMnZn Catalysts.** The particle size of copper oxide on CuZn catalyst is approximately 6.87 nm, as derived from the CuO(111) peak at 38.7° in the XRD pattern of the CuZn catalyst (Figure 1a) and estimated using the Debye−Scherrer formula. However, the CuO peak of CuMnZn is not obvious because some CuO crystallites are highly dispersed or in amorphous form on the catalyst. It is clear that the addition of Mn metal can provide small particle sizes of copper species on the surface.

The catalytic activities of CuZn and CuMnZn in the POM reaction are shown in Figure 2. Both catalysts are in their original oxidation states. The CuZn catalyst displayed a poorer


dx.doi.org/10.1021/ie501023z | Ind. Eng. Chem. Res. 2014, 53, 12622−12630

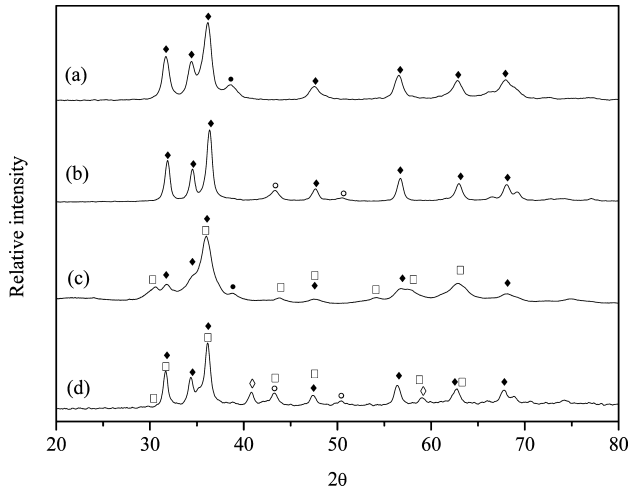


**Figure 1.** X-ray diffraction patterns of (a,b) CuZn and (c,d) CuMnZn catalysts, (a,c) fresh and (b,d) after the POM reaction: (◆) ZnO, (●) CuO, (○) Cu, (◇) MnO, (□) $CuMn_2O_4$.

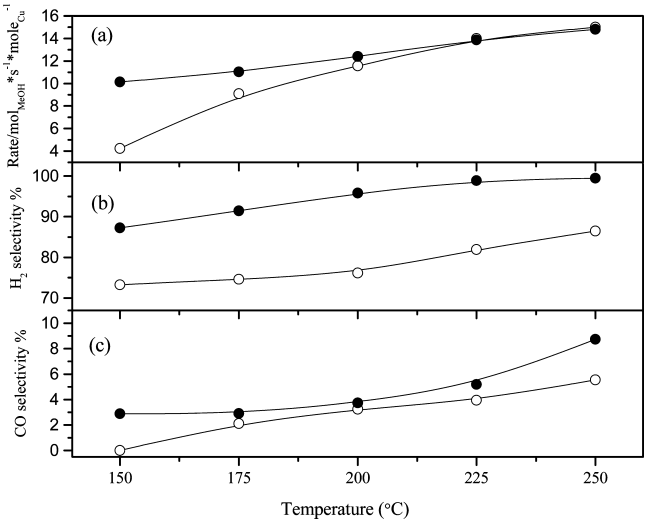


**Figure 2.** (a) Turnover frequency (TOF) for methanol conversion [TOF = (moles of MeOH per gram per second)/(moles of Cu surface per gram)], (b) hydrogen selectivity [$S_{H_2} = n_{H_2}/(n_{H_2} + n_{H_2O}) \times 100\%$], and (c) carbon monoxide selectivity [$S_{CO} = n_{CO}/(n_{CO} + n_{CO_2}) \times 100\%$] as functions of reaction temperature during the POM reaction over (○) CuZn and (●) CuMnZn catalysts.

TOF for methanol conversion and hydrogen formation, especially at lower temperatures (only 4.2 $s^{-1}$ and 73%, respectively, at 150 °C). Compared with CuZn catalyst, CuMnZn catalyst with manganese additive had a significant positive effect. The TOF for methanol conversion was higher than 10 $s^{-1}$ at $T$ > 150 °C, and methanol could be completely converted at $T$ > 250 °C. In the meantime, $S_{H_2}$ remained higher than 90% at $T$ > 175 °C, despite a slightly higher $S_{CO}$ value in this range of reaction temperatures.

The X-ray diffraction patterns of CuZn and CuMnZn catalysts before and after POM reaction are shown in Figure 1. Because of the amorphous nature and nanoscale size of the mixed CuMnO, less crystallinity was observed in fresh CuMnZn (Figure 1c). It is considered that these amorphous phases of copper manganese oxide have a higher activity than the crystalline phases.[1] Some researchers[22,35,36] have suggested that the dispersion of copper would be promoted by incorporating it into the lattice of $Cu_xMn_{3-x}O_4$ spinel structure. After POM treatment (Figure 1b,d), only CuO was reduced to Cu for CuZn catalyst, but the CuMnZn catalyst showed that CuO disappeared and the reduced species of Cu and MnO appeared. In addition, the $CuMn_2O_4$ still existed after the POM reaction over the CuMnZn catalyst but was more crystalline. All XRD peaks of both CuZn and CuMnZn catalysts became shaped. According to the Debye−Scherrer formula, this means that these catalysts aggregated during the POM reaction.

**3.2. Microkinetic Modeling Analysis.** To further realize the surface species or intermediates on the CuMnZn catalysts during the POM reaction, the mechanisms and reaction pathways of the POM reaction were examined by in situ DRIFTS (Figure 3I,II). The IR spectra (Figure 3Ia,b;IIa,b) of the surface species on the catalyst in the POM reaction at both 160 and 180 °C display obvious bands at 2928, 2865, 2820, 1443, and 1060 $cm^{-1}$ that can be assigned as methoxy groups ($CH_3O$*).[37,38] The route for the formation of $CH_3O$* is dehydrogenation from methanol on the catalyst surface. There was also a broad band at 3100−3500 $cm^{-1}$ that can be assigned to hydroxy groups (OH*), implying that the oxygen source reacts with methanol to form OH* groups. Formate groups (HCOO*) appear at 2960, 2870, 2745, and 1600 $cm^{-1}$[39,40] and were formed from the dehydrogenation of methoxy and rapid oxidation of formaldehyde. Formaldehyde was not detected, because of its rapid oxidation into formate species through $OCH_2O$* or CHO* (s6-1, s6-2). According to some of the literature,[26,42,43] the adsorption bands in the region of 1300−1400 $cm^{-1}$ are contributed by the symmetric OCO stretching mode, and those in the 1600−1700 $cm^{-1}$ range are contributed by the asymmetric mode. Thus, the peak at 1600 $cm^{-1}$ can be assigned to monodentate formate, and the peak at 1360 $cm^{-1}$ can be assigned to bidentate formate. Because of no band was observed at 1360 $cm^{-1}$ at 180 °C, the possibility of the formation of monodentate formate through s6-1 is higher than that through s6-2 at lower temperature. Thus, the adsorbed- and surface-reacted pathways can be simplified to the following reaction steps, where * and *l* represent metal and oxide sites, respectively

$$\text{s1:}\quad O_2 + l \rightarrow O_2l \tag{7}$$

$$\text{s2:}\quad O_2l + l \rightarrow 2Ol \tag{8}$$

$$\text{s3:}\quad CH_3OH + l \rightarrow CH_3OHl \tag{9}$$

$$\text{s4:}\quad CH_3OHl + Ol \rightarrow CH_3O^* + OHl \tag{10}$$

$$\text{s5:}\quad CH_3O^* + l \rightarrow CH_2O^* + Hl \tag{11}$$

$$\text{s6-1:}\quad CH_2O^* + Ol \rightarrow OCH_2O^* + l \rightarrow HCOO^* + Hl \quad (T \leq 180\ ^\circ C) \tag{12}$$

$$\text{s6-2:}\quad CH_2O^* + Ol \rightarrow CHO^* + Hl + Ol \rightarrow HCOO^* + Hl \quad (T > 180\ ^\circ C) \tag{13}$$

When the temperature was raised to 200 °C (Figure 3Ic,IIc), all of the characteristic peaks of $CH_3O$* were dramatically reduced (Figure 3IIIb,IVb) because of the violent ignition process and hydrogen generation at millisecond contact times on the catalyst.[41] The consumption of HCOO* implied that formate decomposition produced COO*, CO*, H*l*, or OH*l* species, to generate $H_2$, $H_2O$, $CO_2$, or CO. Interestingly,


dx.doi.org/10.1021/ie501023z | Ind. Eng. Chem. Res. 2014, 53, 12622−12630

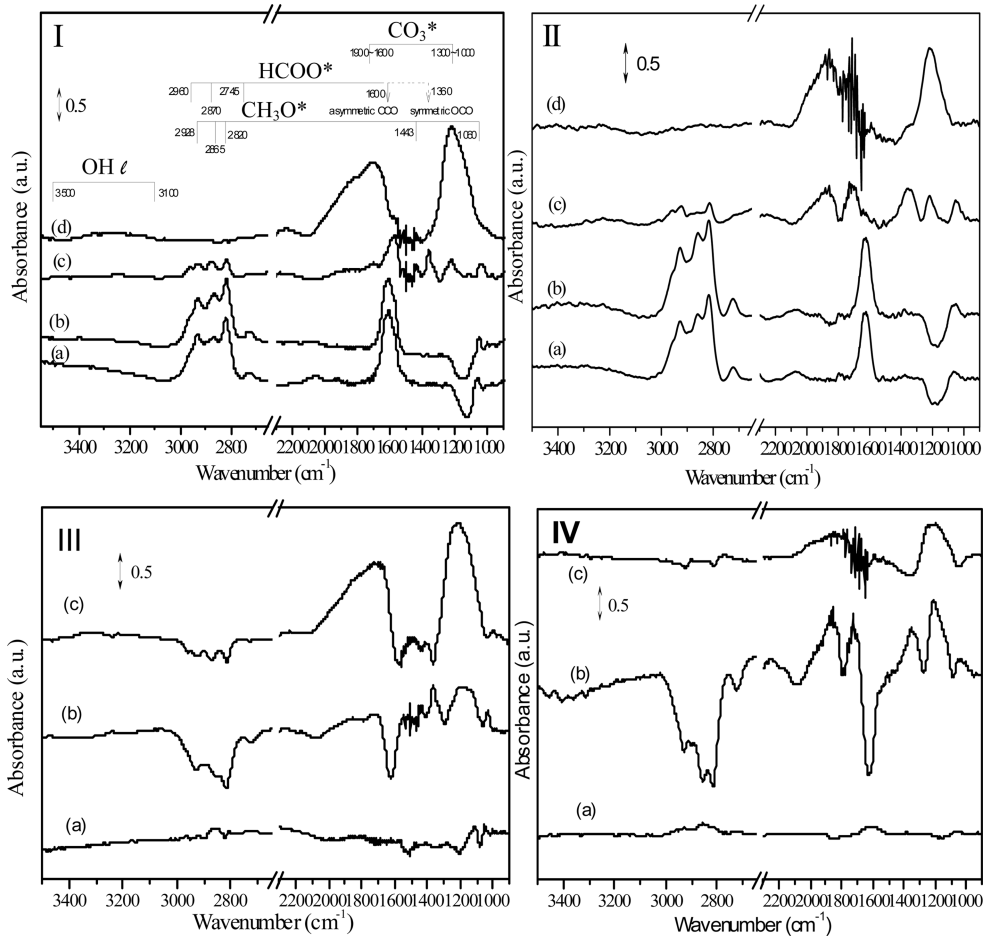


**Figure 3.** In situ DRIFTS spectra of surface species evolution during thermal treatment of methanol/oxygen adsorption on (I) CuZn and (II) CuMnZn catalysts at (a) 160, (b) 180, (c) 200, and (d) 300 °C. Difference plots of surface species on (III) CuZn and (IV) CuMnZn catalysts were obtained by subtracting DRIFT spectra as follows: (a) 160 from 180 °C, (b) 180 from 200 °C, and (c) 200 from 300 °C.

compared with CuZn catalyst, most monodentate formate on CuMnZn was transformed into bidentate formate at high temperatures (>180 °C, shown in Figure 3IIIb,IVb). However, some bands around 1600−1900 and 1000−1300 $cm^{-1}$ can be ascribed to carbonate species that appeared by restricting the motion of oxygen.[44] These more stable carbonate species decompose on the surface with greater difficulty. Accordingly, the pathways might show up as the following reactions

$$\text{s7:}\quad \text{HCOO*} + l \rightarrow \text{H}l + \text{COO*} \tag{14}$$

$$\text{s8:}\quad \text{HCOO*} + l \rightarrow \text{OH}l + \text{CO*} \tag{15}$$

$$\text{s9:}\quad \text{H}l + \text{H}l \rightarrow \text{H}_2l + l \tag{16}$$

$$\text{s10:}\quad \text{H}_2l \rightarrow \text{H}_2(\text{g}) + l \tag{17}$$

$$\text{s11:}\quad \text{H}l + \text{OH}l \rightarrow \text{H}_2\text{O}l + l \tag{18}$$

$$\text{s12:}\quad \text{H}_2\text{O}l \rightarrow \text{H}_2\text{O}(\text{g}) + l \tag{19}$$

$$\text{s13:}\quad \text{COO*} \rightarrow \text{CO}_2(\text{g}) + * \tag{20}$$

$$\text{s14:}\quad \text{CO*} \rightarrow \text{CO}(\text{g}) + * \tag{21}$$

$$\text{s15:}\quad \text{HCOO*} + \text{O}l \rightarrow \text{CO}_3* + \text{H}l \tag{22}$$

With a further increase in temperature to ∼300 °C (Figure 3Id,IId), methoxy and bidentate formate were consumed completely (Figure 3IIIc,IVc), and the total adsorbed species were decomposed violently and desorbed quickly from the surface.

The whole reaction mechanism and probable pathways for POM on the predominant sites of CuMnZn catalyst are proposed and presented in Figure 4. Methoxy and monodentate formate must dominate below the ignition temperature (≤180 °C). However, when the catalyst reaches ignition temperature (>180 °C), the strength of the C−H stretching bond is dramatically reduced because of turbulent hydrogenation. The results show that the formate species is the important intermediate during the POM reaction; that it would further decompose to $CO_2$, CO, H, or OH adsorption species on the surface; and that these species would then finally desorb. Some carbonate species ($CO_3$*) would be generated from the oxidation of formate at high reaction temperatures (200−300 °C) on the catalyst surface.

Notice that, compared with the CuZn catalyst, more carbonate species were formed on the CuMnZn catalyst at 200 °C (Figure 3IVb), which exhibited more oxygen trapped on the surface of the CuMnZn catalyst. However, at higher temperature, the existence of the CuMnZn spinel structure should play an important role in improving the movement of oxygen. Thus, the accumulation of carbonate species was mitigated. By contrast, without the assistance of manganese promoter, the accumulation of carbonate species becomes very severe on CuZn catalyst at high temperature. Moreover, the


dx.doi.org/10.1021/ie501023z | Ind. Eng. Chem. Res. 2014, 53, 12622−12630

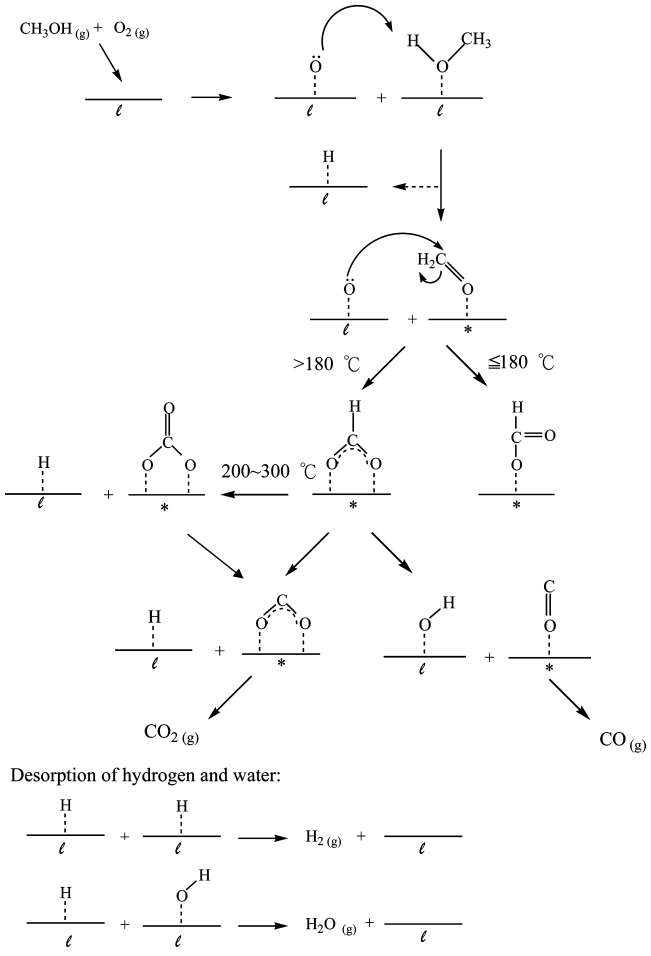


**Figure 4.** Proposed reaction mechanisms for POM over CuMnZn catalyst. * and *l* represent metal and oxide sites, respectively, on the catalyst surface.

durability of the CuZn catalysts with and without Mn promoter in the POM reaction at 350 °C is shown in Figure 5. Compared with the dramatic decay of CuZn catalyst (25% loss after 72 h), CuMnZn catalyst maintained higher catalytic activity (TOF = 15 $s^{-1}$ within 72 h) and slightly better stability. The durability of CuZn catalyst was obviously improved by use of the Mn promoter, which mitigated the accumulation of carbonate species.

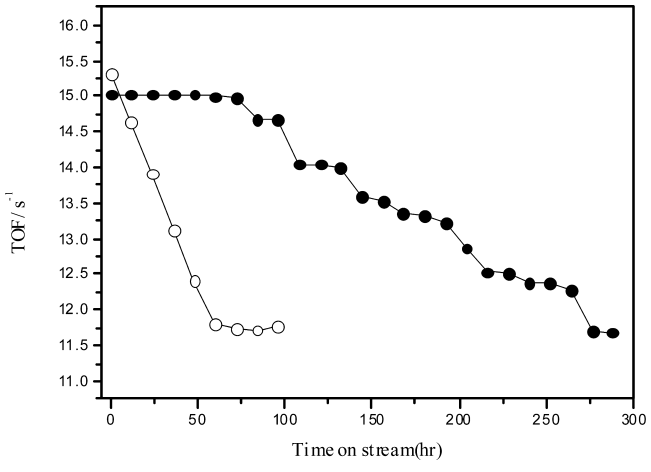


**Figure 5.** Time-on-stream stability tests of the (○) CuZn and (●) CuMnZn catalysts in the POM reaction at 350 °C. The TOF is in (moles of MeOH per gram per second)/(moles of Cu surface per gram).

To further understand the role of Mn in the CuMnZn catalyst during the POM reaction at high temperature, the variations in the electrically charged states of copper and manganese species with time on stream during the POM at 350 °C were observed by in situ XAS. The Cu K-edge jump energy according to X-ray absorption near-edge structure (XANES) spectroscopy (Figure 6a) was 8979 eV, and the edge feature at 8981−8984 eV was attributed to the dipole-allowed 1s-to-4p transition of $Cu^{2+}$ that occurred through the oxidation of $Cu^0$.[45] The peak appearing between 8975 and 8982 eV can be assigned to the transition from the 1s to the 3d orbital.[46] Table 1 also shows that most of the $Cu^{2+}$ in the fresh CuMnZn catalyst was reduced to 32.1% $Cu^0$ and 64.4% $Cu^+$ in the initial reaction, and then the maximum $Cu^0$ species was achieved at 24 h (78.7%). However, the amount of $Cu^{2+}$ increased with time during the POM reaction. Many studies indicate that $Cu^{2+}$ is inactive,[1,5,7,12,47] resulting in gradual catalytic deactivation during the POM reaction. In summary, during the POM reaction, copper species varied with the reduction−oxidation mechanism $Cu^{2+} \rightarrow Cu^+ + Cu^0 \rightarrow Cu^{2+}$. First, methanol was adsorbed on the surface of the fresh catalyst, and then the formation of methoxy or formate might induce the reduction of the $Cu^{2+}$ to $Cu^+$ and $Cu^0$. Another work also proposed that $Cu^0$ is involved in the formation of $CO_2$ and $H_2$. $Cu^+$ sites favor the formation of CO and $H_2O$, and $Cu^{2+}$ is relatively inactive in the POM.[1] Over time, a large volume of oxygen was diffused into the lattice of copper species, and the content of $Cu^{2+}$ increased. The accumulation of carbonic species might have also blocked the active sites. The catalysts deactivated gradually.

Figure 6b shows the Mn K-edge XANES result . The Mn K-edge jump energy according to XANES spectroscopy (Figure 6a) was 6539 eV.[48,49] For fresh CuMnZn, ca. 58% $Mn^{4+}$ ($MnO_2$) and 42% $Mn^{8/3+}$ were observed, and then most of manganese species were reduced to 1−4% $Mn^{3+}$ ($Mn_2O_3$), 29−35% $Mn^{8/3+}$ ($Mn_3O_4$), and 60−68% $Mn^{2+}$ (MnO) during POM treatment. Because of the irregular variations in the percentages of manganese species (Table 1) during time on stream, Mn species should play a role in electronic charge transfer, which allows the rapid storage and release of electrons and promotes the movement of oxygen. This might be the reason that the accumulation of carbonate species can be mitigated.

From previous statements, we found that the performance of CuZn catalyst can be enhanced at low temperature by adding manganese promoter. Kinetic modeling analysis was used to further understand the diversity of activation energy and Arrhenius coefficient of POM reaction over CuMnZn catalyst. To follow the mass balance principle, kinetic modeling analysis of CuMnZn was performed in the range of 160−190 °C. Panels a−d of Figure 7 display the mole fractions of components of the product as a function of contact time at modeling temperatures of 160, 170, 180, and 190 °C, respectively. Ultralow CO was generated (>1%) even at relatively low temperatures, so this product was ignored in the kinetic modeling analysis. Moreover, the KN criterion test (Figure S1 in the Supporting Information) shows that the reactions obeyed the KN criteria, so the reactions were carried out in the absence of mass- and heat-transfer limitations.

Determination of the rate-determining step and rate constants was accomplished by fitting the simulated model to


dx.doi.org/10.1021/ie501023z | Ind. Eng. Chem. Res. 2014, 53, 12622−12630

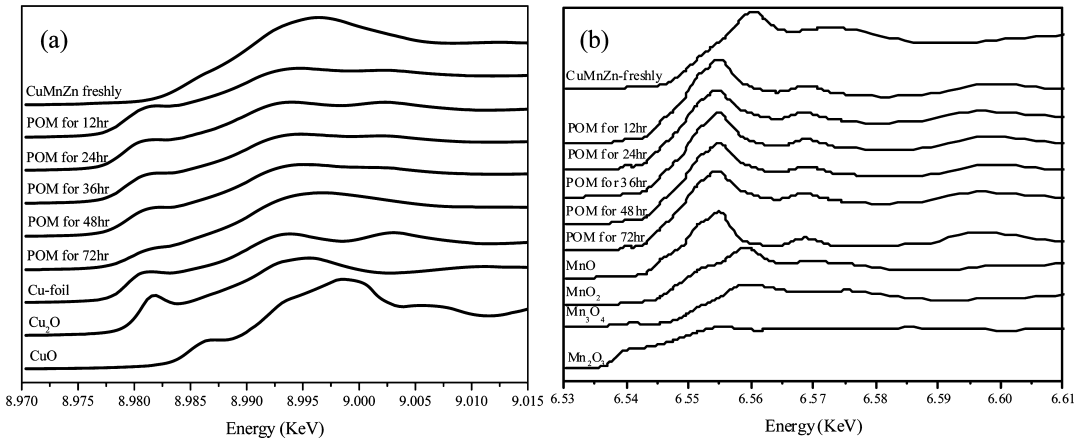


**Figure 6.** In situ XANES spectra of the CuMnZn catalyst during time-on-stream for POM: (a) Cu K-edge and (b) Mn K-edge. XANES spectra of Cu foil, $Cu_2O$, CuO, MnO, $MnO_2$, $Mn_3O_4$, and $Mn_2O_3$ are included for comparison.

**Table 1. Percentages of Copper and Manganese Species in CuMnZn Catalyst by in Situ XANES Data Fitting**

| | Cu species (%) | | | Mn species (%) | | | |
|---|---|---|---|---|---|---|---|
| sample | $Cu^{2+}$ | $Cu^{+}$ | $Cu^{0}$ | $Mn^{4+}$ | $Mn^{3+}$ | $Mn^{8/3+}$ | $Mn^{2+}$ |
| fresh | 100 | 0 | 0 | 58.1 | 0 | 41.9 | 0 |
| POM for 12 h | 3.5 | 32.1 | 64.4 | 0 | 1.7 | 29.4 | 68.9 |
| POM for 24 h | 2.4 | 18.9 | 78.7 | 0 | 2.4 | 32.4 | 65.2 |
| POM for 36 h | 7.7 | 28.5 | 63.8 | 0 | 3.4 | 35.8 | 60.8 |
| POM for 48 h | 15.9 | 28.6 | 55.5 | 0 | 2.5 | 28.2 | 69.3 |
| POM for 72 h | 18.5 | 37.1 | 44.4 | 0 | 4.2 | 34.3 | 61.5 |

all of the measured data. Table 2 summarizes plausible pathways and rate equations. Those feasible pathways were set by the graph-theoretic method based on P-graphs.[50−53] Independent pathways were lumped into six steps comprising adsorption [including $O_2$ and MeOH chemisorptions (s1 + s2 and s3)]; surface reaction (s4 + s5 + s6-1/s6-2 + s7 + s9 + s11); and $H_2$, $H_2O$, and $CO_2$ desorption (s10, s12, and s13). The kinetic rate expression was obtained by the LHHW formalism,[54] which takes into account all active sites on the catalyst surface and derives the rate equation by assuming that one of the pathways (e.g., surface reaction) is the rate-

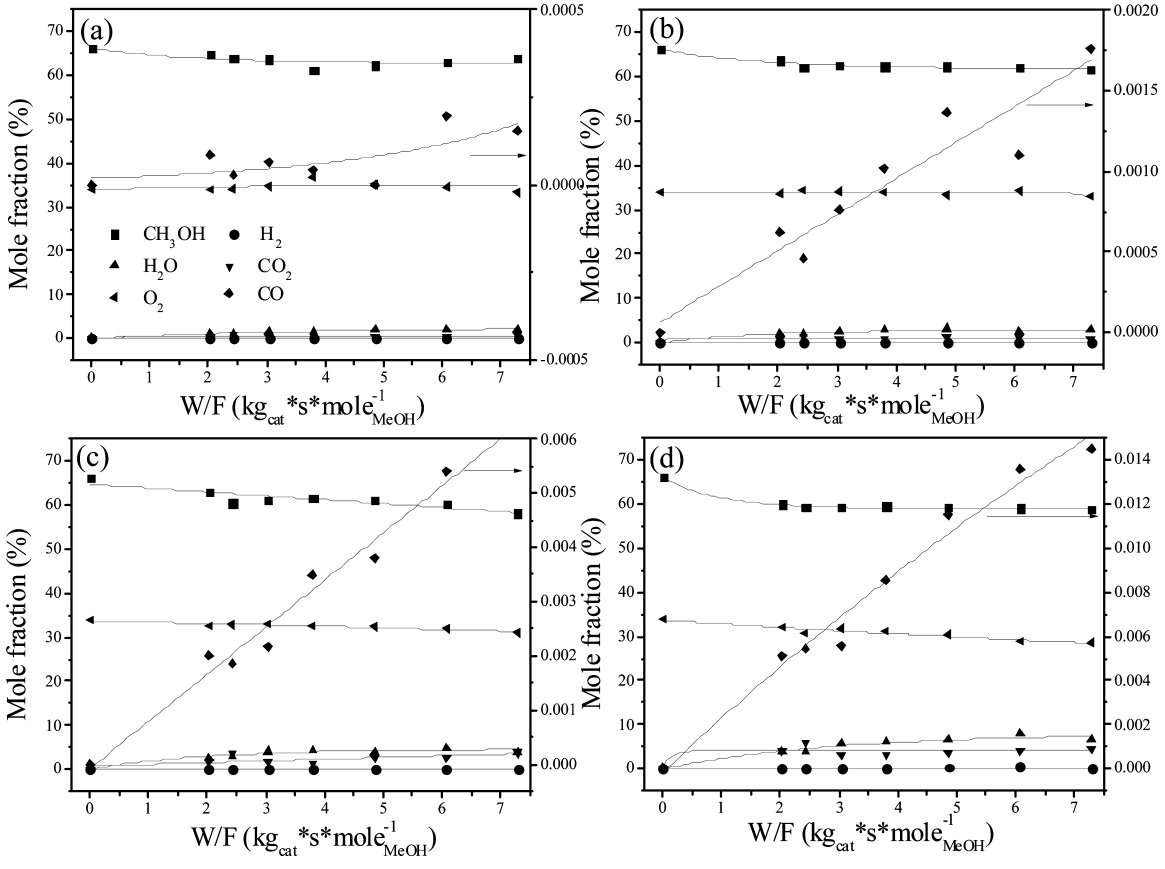


**Figure 7.** Mole fractions of components in the product as a function of contact time at (a) 160, (b) 170, (c) 180, and (d) 190 °C.


dx.doi.org/10.1021/ie501023z | Ind. Eng. Chem. Res. 2014, 53, 12622−12630

**Table 2. Lumped Reaction Steps of POM over CuMnZn Catalyst**

| | designation | reaction step[a] |
|---|---|---|
| oxygen adsorption (s1 + s2) | ad,1 | $O_2 + 2l \xrightarrow{K_{ad,1}} 2Ol$ |
| methanol adsorption (s3) | ad,2 | $CH_3OH + l \xrightarrow{K_{ad,2}} CH_3OHl$ |
| surface reaction (s4 + s5 + s6-1/s6-2 + s7 + s9 + s11) | sf | $CH_3OHl + 2Ol \xleftrightarrow{K_{sf}} CO_2* + H_2Ol + H_2l$ |
| carbon dioxide desorption (s13) | de,1 | $CO_2* \xleftrightarrow{K_{de,1}} CO_2 + *$ |
| water desorption (s10) | de,2 | $H_2Ol \xrightarrow{K_{de,2}} H_2O + l$ |
| hydrogen desorption (s12) | de,3 | $H_2l \xrightarrow{K_{de,3}} H_2 + l$ |

[a] * and *l* represent metal and oxide sites, respectively.

**Table 3. Comparing the Activation Energies of POM over CuZn-Based Catalysts**

| catalyst | $E_a$ (kcal mol$^{-1}$) | $T_r$ range (°C) | ref |
|---|---|---|---|
| $Cu_{30}Zn_{70}$ | 115 | 200−230 | 1 |
| $Cu_{70}Zn_{30}$ | 17 | 200−230 | 1 |
| $Cu_{70}Zn_{30}$ | 15.1 | 30−300 | 52 |
| $Cu_{40}Zn_{45}Al_{15}$ | 20 | 200−230 | 1 |
| $Cu_{40}Zn_{50}Al_{10}$ | 20 | 200−230 | 1 |
| $Cu_{40}Zn_{55}Al_5$ | 54 | 200−230 | 1 |
| $Pd_1-Cu_{70}Zn_{30}$ | 13.4 | 30−300 | 52 |
| $Cu_{29.2}Zn_{70.8}$ | 22.4 | 170−200 | this study |
| $Cu_{28.0}Mn_{23.3}Zn_{48.7}$ | 16.5 | 160−190 | this study |

determining state, whereas the remaining pathways are in equilibrium states.[7,54]

Figure 8a shows an Arrhenius plot of the rate constant $k_{sf}$. By calculating the slope and intercept of the linear trend of the Arrhenius plot, the activation energy and pre-exponential factor were found to be 16.5 kcal/mol and $5.26 \times 10^8$, respectively. Figure 8b shows a parity plot between the experimentally determined reaction rate and the value obtained based on the simplified rate equation for surface reaction. The experimental and estimated values are in excellent agreement. Moreover, assuming $r_{de,1}$ (carbon dioxide desorption) as the rate-determining step, other kinetic parameter values were obtained (see Supporting Information, sections II−IV). The Arrhenius plot of the rate constant $k_{de,1}$ and the parity plot are shown in section V of the Supporting Information. The activation energy and pre-exponential factor for $r_{de,1}$ were found to be 52.2 kcal/mol and $5.62 \times 10^{18}$, respectively. Note that the activation energies for $r_{sf}$ and $r_{de,1}$ differ significantly: The former is 16.5 kcal/mol, and the latter is 52.2 kcal/mol. Hence, the surface reaction between chemisorbed methanol and oxygen to bidentate formate is more likely to be the rate-determining step in POM than the carbon dioxide desorption step. It is noteworthy that the activation energy of POM has been estimated in several reports in the literature (see Table 3). Alejo et al.[1] showed that $Cu_{30}Zn_{70}$ catalyst had a high activation energy of about 115 kcal mol$^{-1}$, whereas the activation energy decreased to 17 kcal mol$^{-1}$ when the copper content was increased to 70%; however, the apparent activation energies obtained in the presence of the $Cu_{40}Zn_{50}Al_{10}$ and $Cu_{40}Zn_{45}Al_{15}$ catalysts were similar at about 20 kcal mol$^{-1}$. Schuyten et al.[55] also showed that the energy of activation was in the range of 15−13 kcal mol$^{-1}$ over $Pd-Cu_{30}Zn_{70}$ catalyst. Additionally, Andreasen et al.[56] demonstrated that the pre-exponential factor of the methanol oxidation microkinetic model for gas-phase molecules falls within the range of $10^9-10^{10}$. Deshmukh et al.[57] reported that the pre-exponential factor was around $10^1$ and $10^9$ for the partial oxidation of methanol to form dimethyl ether and dimethoxymethane, respectively. Consequently, the results imply that surface reaction between chemisorbed methanol and oxygen to bidentate formate is more applicable than carbon dioxide desorption as the rate-determining step.

In addition, the same kinetic modeling analysis, assuming surface reaction as the rate-determining step for CuZn standard catalyst, was also performed (see Supporting Information, section VI). The values of $E_a$ = 22.4 kcal/mol and pre-exponential = $2.11 \times 10^{10}$ were obtained. In comparing CuZn-based catalysts (Table 3), the addition of manganese was found to lower $E_a$ from 22.4 to 16.5 kcal/mol during the POM reaction at 180 °C. In this study, the POM reaction could be accelerated after the decomposition of formate (Figures 2a and 3IIIb,IVb). Moreover, more bidentate formate was observed on

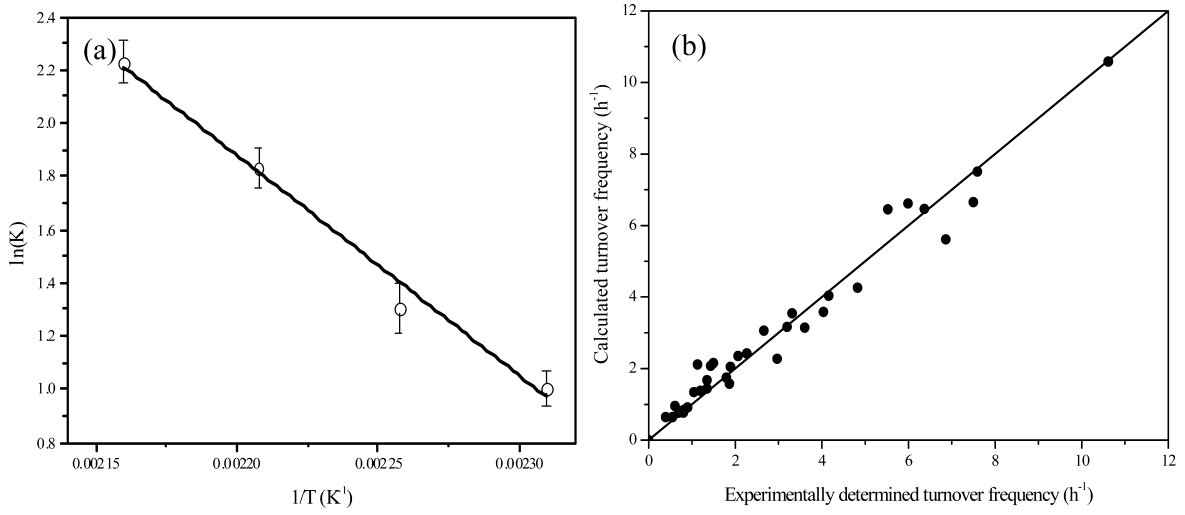


**Figure 8.** (a) Arrhenius plot of CuMnZn catalyst based on the assumption that the surface reaction was the rate-determining step. (b) Parity plot of the reaction rate for CuMnZn catalyst.

CuMnZn catalyst, and the accumulation of carbonate species was mitigated at high temperature. Accordingly, manganese also provides an electronic transmitter to transfer electrons easily. This indicates that the existence of the CuMnZn spinel structure should play an important role in improving the movement of oxygen and simultaneously enhancing the performance of the POM reaction.

## 4. CONCLUSIONS

CuZn-based catalyst, promoted with Mn, can effectively enhance the TOF for methanol conversion to 10.1 $s^{-1}$ at 150 °C. For the POM reaction, copper species varied within a reduction−oxidation mechanism of $Cu^{2+} \rightarrow Cu^{+} + Cu^{0} \rightarrow Cu^{2+}$. Mn could provide an electronic transmitter to promote the storage and release of electrons. Simultaneously, more bidentate formate and carbonate species were formed on CuMnZn catalyst at 200 °C and tended to mitigate at high temperature. In comparison with previous studies, the apparent activation energy (16.5 kcal/mol) in this study was lower than that for a general CuZn-based standard catalyst (22.4 kcal/mol). The existence of the CuMnZn spinel structure should play an important role in accelerating formate decomposition and improving the movement of oxygen.

## ■ ASSOCIATED CONTENT

### Supporting Information

Derivation of the rate equation, mechanistic rate equations, kinetic parameters of the simplified rate equation, and Arrhenius plot and parity plot of the reaction rate for catalysts. This material is available free of charge via the Internet at http://pubs.acs.org.

## ■ AUTHOR INFORMATION

### Corresponding Author

*Tel.: +88635715131 ext 35496. Fax: +88635718649. E-mail: yjhuang@mx.nthu.edu.tw.

### Notes

The authors declare no competing financial interest.

## ■ ACKNOWLEDGMENTS

The authors are grateful for the financial support of this work from the Ministry of Science and Technology of Taiwan. We also thank Dr. Hwo-Shuenn Sheu and Dr. Yu-Chun Chuang, BL01C2 spokespersons, and Dr. Jyh-Fu Lee, Beamline 17C spokesperson, at the National Synchrotron Radiation Center, Taiwan, for assisting in the XRD and XAS experiments, respectively. Thanks are also offered to Editor Prof. Linda J. Broadbelt and three anonymous reviewers for their comments.

## ■ REFERENCES

(1) Alejo, L.; Lago, R.; Pena, M. A.; Fierro, J. L. G. Partial oxidation of methanol to produce hydrogen over Cu−Zn-based catalysts. *Appl. Catal. A: Gen.* **1997**, *162*, 281.

(2) Velu, S.; Suzuki, K.; Osaki, T. Selective production of hydrogen by partial oxidation of methanol over catalysts derived from CuZnAl-layered double hydroxides. *Catal. Lett.* **1999**, *62*, 159.

(3) Agrell, J.; Hasselbo, K.; Jansson, K.; Jaras, S. G.; Boutonnet, M. Production of hydrogen by partial oxidation of methanol over Cu/ZnO catalysts prepared by microemulsion technique. *Appl. Catal. A: Gen.* **2001**, *211*, 239.

(4) Agrell, J.; Boutonnet, M.; Melian-Cabrera, I.; Fierro, J. L. G. Production of hydrogen from methanol over binary Cu/ZnO catalysts: Part I. Catalyst preparation and characterisation. *Appl. Catal. A: Gen.* **2003**, *253*, 201.

(5) Agrell, J.; Boutonnet, M.; Fierro, J. L. G. Production of hydrogen from methanol over binary Cu/ZnO catalysts: Part II. Catalytic activity and reaction pathways. *Appl. Catal. A: Gen.* **2003**, *253*, 213.

(6) Espinosa, L. A.; Lago, R. M.; Pena, M. A.; Fierro, J. L. G. Mechanistic aspects of hydrogen production by partial oxidation of methanol over Cu/ZnO catalysts. *Top Catal.* **2003**, *22*, 245.

(7) Lin, Y. C.; Fan, L. T.; Shafie, S.; Hohn, K. L.; Bertok, B.; Friedler, F. Catalytic pathways identification for partial oxidation of methanol on copper−zinc catalysts: $CH_3OH + 1/2O_2 \leftrightarrow CO_2 + 2H_2$. *Ind. Eng. Chem. Res.* **2008**, *47*, 2523.

(8) Tang, H. Y.; Erickson, P.; Yoon, H. C.; Liao, C. H. Comparison of steam and autothermal reforming of methanol using a packed-bed low-cost copper catalyst. *Int. J. Hydrogen Energy* **2009**, *34*, 7656.

(9) Wang, Z. F.; Xi, J. Y.; Wang, W. P.; Lu, G. X. Selective production of hydrogen by partial oxidation of methanol over Cu/Cr catalysts. *J. Mol. Catal. A: Chem.* **2003**, *191*, 123.

(10) Cubeiro, M. L.; Fierro, J. L. G. Selective production of hydrogen by partial oxidation of methanol over ZnO-supported palladium catalysts. *J. Catal.* **1998**, *179*, 150.

(11) Mo, L. Y.; Zheng, X. M.; Yeh, C. T. Selective production of hydrogen from partial oxidation of methanol over silver catalysts at low temperatures. *Chem. Commun.* **2004**, *12*, 1426.

(12) Huang, Y. J.; Ng, K. L.; Huang, H. Y. The effect of gold on the copper-zinc oxides catalyst during the partial oxidation of methanol reaction. *Int. J. Hydrogen Energy* **2011**, *36*, 15203.

(13) Jansen, W. P. A.; Beckers, J.; van der Heuvel, J. C.; van der Gon, A. W. D.; Bliek, A.; Brongersma, H. H. Dynamic behavior of the surface structure of $Cu/ZnO/SiO_2$ catalysts. *J. Catal.* **2002**, *210*, 229.

(14) Yoshihara, J.; Campbell, C. T. Methanol synthesis and reverse water−gas shift kinetics over Cu(110) model catalysts: Structural sensitivity. *J. Catal.* **1996**, *161*, 776.

(15) Wilmer, H.; Hinrichsen, O. Dynamical changes in $Cu/ZnO/Al_2O_3$ catalysts. *Catal. Lett.* **2002**, *82*, 117.

(16) Lin, S. D.; Hsiao, T. C.; Chen, L. C. The steady state methanol decomposition reaction over Cu/Zn and Cu/Cr catalysts: Pretreatment, operando EXAFS, and activity study. *Appl. Catal. A: Gen.* **2009**, *360*, 226.

(17) Craciun, R.; Nentwick, B.; Hadjiivanov, K.; Knozinger, H. Structure and redox properties of $MnO_x$/yttrium-stabilized zirconia (YSZ) catalyst and its use in CO and $CH_4$ oxidation. *Appl. Catal. A: Gen.* **2003**, *243*, 67.

(18) Morales, M. R.; Barbero, B. P.; Cadus, L. E. Total oxidation of ethanol and propane over Mn-Cu mixed oxide catalysts. *Appl. Catal. B* **2006**, *67*, 229.

(19) Hutchings, G. J.; Mirzaei, A. A.; Joyner, R. W.; Siddiqui, M. R. H.; Taylor, S. H. Effect of preparation conditions on the catalytic performance of copper manganese oxide catalysts for CO oxidation. *Appl. Catal. A: Gen.* **1998**, *166*, 143.

(20) Gottschalk, F. M.; Hutchings, G. J. Manganese oxide water−gas shift catalysts initial optimization studies. *Appl. Catal.* **1989**, *51*, 127.

(21) Hutchings, G. J.; Copperthwaite, R. G.; Gottschalk, F. M.; Hunter, R.; Mellor, J.; Orchard, S. W.; Sangiorgio, T. A comparative evaluation of cobalt chromium oxide, cobalt manganese oxide, and copper manganese oxide as catalysts for the water−gas shift reaction. *J. Catal.* **1992**, *137*, 408.

(22) Papavasiliou, J.; Avgouropoulos, G.; Ioannides, T. Steam reforming of methanol over copper−manganese spinel oxide catalysts. *Catal. Commun.* **2005**, *6*, 497.

(23) Papavasiliou, J.; Avgouropoulos, G.; Ioannides, T. Combined steam reforming of methanol over Cu−Mn spinel oxide catalysts. *J. Catal.* **2007**, *251*, 7.

(24) Kanungo, S. B. Physicochemical properties of $MnO_2$ and $MnO_2$−CuO and their relationship with the catalytic activity for $H_2O_2$ decomposition and CO oxidation. *J. Catal.* **1979**, *58*, 419.

(25) Figueroa, S. J. A.; Requejo, F. G.; Lede, E. J.; Lamaita, L.; Peluso, M. A.; Sambeth, J. E. XANES study of electronic and structural nature

of Mn sites in manganese oxides with catalytic properties. *Catal. Today* **2005**, *107−08*, 849.
(26) Cao, C. D.; Hohn, K. L. Study of reaction intermediates of methanol decomposition and catalytic partial oxidation on $Pt/Al_2O_3$. *Appl. Catal. A: Gen.* **2009**, *354*, 26.
(27) Peppley, B. A.; Amphlett, J. C.; Kearns, L. M.; Mann, R. F. Methanol steam reforming on $Cu/ZnO/Al_2O_3$ catalysts. Part 2. A comprehensive kinetic model. *Appl. Catal. A: Gen.* **1999**, *179*, 31.
(28) Fisher, I. A.; Bell, A. T. A mechanistic study of methanol decomposition over $Cu/SiO_2$, $ZrO_2/SiO_2$, and $Cu/ZrO_2/SiO_2$. *J. Catal.* **1999**, *184*, 357.
(29) Bianchi, D.; Chafik, T.; Khalfallah, M.; Teichner, S. J. Intermediate Species on Zirconia Supported Methanol Aerogel Catalysts V. Adsorption of Methanol. *Appl. Catal. A: Gen.* **1995**, *123*, 89.
(30) Huang, T. J.; Chren, S. L. Kinetics of Partial Oxidation of Methanol over a Copper−Zinc Catalyst. *Appl. Catal.* **1988**, *40*, 43.
(31) J.J, C. *Chemical and Catalytic Reaction Engineering*, 3rd ed.; McGraw-Hill: New York, 1976.
(32) Madon, R. J.; Boudart, M. Experimental criterion for absence of artifacts in the measurement of rates of heterogeneous catalytic reactions. *Ind. Eng. Chem. Fundam* **1982**, *21*, 438−447.
(33) Kumar, D.; Ali, A. Nanocrystalline K−CaO for the trans-esterification of a variety of feedstocks: Structure, kinetics and catalytic properties. *Biomass Bioenergy* **2012**, *46*, 459−468.
(34) Stewart, W. E.; Caracotsios, M.; Sorensen, J. P. Parameter Estimation from Multiresponse Data. *AIChE J.* **1992**, *38*, 641.
(35) PalDey, S.; Gedevanishvili, S.; Zhang, W.; Rasouli, F. Evaluation of a spinel based pigment system as a CO oxidation catalyst. *Appl. Catal. B* **2005**, *56*, 241.
(36) Papavasiliou, J.; Avgouropoulos, G.; Ioannides, T. In situ combustion synthesis of structured Cu−Ce−O and Cu−Mn−O catalysts for the production and purification of hydrogen. *Appl. Catal. B* **2006**, *66*, 168.
(37) Millar, G. J.; RRochester, C. H.; Waugh, K. C. Evidence for the adsorption of molecules at special sites located at copper−zinc oxide interfaces: Part 2. A Fourier-Transform Infrared Spectroscopy Study of Methanol Adsorption on Reduced and Oxidized $Cu/Zno/SiO_2$ Catalysts. *J. Chem. Soc. Faraday T.* **1992**, *88*, 2257.
(38) Camplin, J. P.; McCash, E. M. A RAIRS study of methoxy and ethoxy on oxidised Cu(100). *Surf. Sci.* **1996**, *360*, 229.
(39) Wovchko, E. A.; Camp, J. C.; Glass, J. A.; Yates, J. T. Active Sites on $SiO_2$: Role in $CH_3OH$ Decomposition. *Langmuir* **1995**, *11*, 2592.
(40) Finocchio, E.; Busca, G. Characterization and hydrocarbon oxidation activity of coprecipitated mixed oxides $Mn_3O_4/Al_2O_3$. *Catal. Today* **2001**, *70*, 213.
(41) Traxel, B. E.; Hohl, K. L. Partial oxidation of methanol at millisecond contact times. *Appl. Catal. A: Gen.* **2003**, *244*, 129.
(42) Gopal, P. G.; Schneider, R. L.; Watters, K. L. Evidence for Production of Surface Formate upon Direct Reaction of Co with Alumina and Magnesia. *J. Catal.* **1987**, *105*, 366.
(43) Cant, N. W.; Little, L. H. Lewis and Bronsted Acid Sites on Silica-Alumina. *Nature* **1966**, *211*, 69.
(44) Lee, K. Y.; Huang, Y. J. Low CO generation on tunable oxygen vacancies of non-precious metallic Cu/ZnO catalysts for partial oxidation of methanol reaction. *Appl. Catal. B: Environ.* **2014**, *150−151C*, 506.
(45) Choi, E. Y.; Nam, I. S.; Kim, Y. G.; Chung, J. S.; Lee, J. S.; Nomura, M. An X-ray Absorption Study of Copper-Ion Exchanged H-Mordenite for Selective Catalytic Reduction of NO by Ammonia. *J. Mol. Catal.* **1991**, *69*, 247.
(46) Kau, L. S.; Hodgson, K. O.; Solomon, E. I. X-ray Absorption Edge and EXAFS Study of the Copper Sites in ZnO Methanol Synthesis Catalysts. *J. Am. Chem. Soc.* **1989**, *111*, 7103.
(47) Agrell, J.; Birgersson, H.; Boutonnet, M.; Melian-Cabrera, I.; Navarro, R. M.; Fierro, J. L. G. Production of hydrogen from methanol over Cu/ZnO catalysts promoted by $ZrO_2$ and $Al_2O_3$. *J. Catal.* **2003**, *219*, 389.
(48) Stueben, B. L.; Cantrelle, B.; Sneddon, J.; Beck, J. N. Manganese K-edge XANES studies of Mn speciation in Lac des Allemands as a function of depth. *Microchem. J.* **2004**, *76*, 113.
(49) de Vries, A. H.; Hozoi, L.; Broer, R. Origin of the chemical shift in X-ray absorption near-edge spectroscopy at the Mn K-edge in manganese oxide compounds. *Int. J. Quantum Chem.* **2003**, *91*, 57.
(50) Friedler, F.; Tarjan, K.; Huang, Y. W.; Fan, L. T. Graph-theoretic approach to process synthesis: Axioms and theorems. *Chem. Eng. Sci.* **1992**, *47*, 1973.
(51) Friedler, F.; Tarjan, K.; Huang, Y. W.; Fan, L. T. Graph-theoretic approach to process synthesis: Polynomial algorithm for maximal structure generation. *Comput. Chem. Eng.* **1993**, *17*, 929.
(52) Fan, L. T.; Bertók, B.; Friedler, F.; Shafie, S. Mechanisms of ammonia-synthesis reaction revisited with the aid of a novel graph-theoretic method for determining candidate mechanisms in deriving the rate law of a catalytic reaction. *Hung. J. Ind. Chem.* **2001**, *29*, 71.
(53) Fan, L. T.; Bertók, B.; Friedler, F. A graph-theoretic method to identify candidate mechanisms for deriving the rate law of a catalytic reaction. *Comput. Chem.* **2002**, *26*, 265.
(54) Jiang, B. S.; Chang, R.; Lin, Y. C. Partial Oxidation of Ethanol to Acetaldehyde over $LaMnO_3$-Based Perovskites: A Kinetic Study. *Ind. Eng. Chem. Res.* **2013**, *52*, 37.
(55) Schuyten, S.; Guerrero, S.; Miller, J. T.; Shibata, T.; Wolf, E. E. Characterization and oxidation states of Cu and Pd in $Pd−CuO/ZnO/ZrO_2$ catalysts for hydrogen production by methanol partial oxidation. *Appl. Catal. A: Gen.* **2009**, *352*, 133.
(56) Andreasen, A.; Lynggaard, H.; Stegelmann, C.; Stoltze, P. A microkinetic model of the methanol oxidation over silver. *Surf. Sci.* **2003**, *544*, 5.
(57) Deshmukh, S. A. R. K.; Annaland, A. V. S.; Kuipers, J. A. M. Kinetics of the partial oxidation of methanol over a Fe−Mo catalyst. *Appl. Catal. A: Gen.* **2005**, *289*, 240.